High Resolution Laser Diagnostics in Millimeter-Scale Micro Pulsed Plasma Thrusters

Erik L. Antonsen*
Rodney L. Burton**
University of Illinois at Urbana-Champaign IL 61801
eantonse@uiuc.edu

Gregory G. Spanjers‡
AFRL Propulsion Directorate, Edwards AFB CA 93524

IEPC-01-157

A class of Micro-Pulsed Plasma Thruster (MicroPPT) is being developed by the Air Force Research Laboratory to provide precise attitude control and stationkeeping ability to 25-kg class satellites. Operating by means of a surface discharge across a Teflon™ propellant fuel bar only a few millimeters in diameter, the MicroPPT delivers a thrust-to-power ratio of 5 - 10 μN-s/J. Due to the low pulse energy and size, the MicroPPT produces a spatially confined and diffuse plasma plume that is difficult to analyze with material probes for validation of plume modeling. To this end, a Herriott Cell interferometer is introduced to measure the plume electron and neutral densities. By focusing a large number of laser beams into a small measurement volume, the Herriott Cell can increase the instrument resolution by a factor of about 10, compared to a single-pass interferometer, with minimal degradation of spatial resolution. Comparison of these results with a 2-color, 2-pass interferometer demonstrates experimental validity of the point measurement technique used. Comparison of the measured electron density with modeling predictions by Keidar and Boyd shows close agreement. Attempts to measure the MicroPPT neutral density with a 2-color configuration of the Herriott Cell interferometer were inconclusive, in spite of previous successes using this technique on larger PPTs.

Introduction

With the increasing presence of micro-propulsion options for spacecraft attitude control and propulsion, there is a corresponding need for the development of experimental techniques to validate modeling efforts geared towards describing the operating physics of these devices. The Air Force Research Laboratory is currently developing a class of Micro-Pulsed Plasma Thrusters (MicroPPTs) using Teflon™ propellant to provide precise impulse bits in the 10 μN-s range. In the near term, these thrusters can provide propulsive attitude control on 150-kg class spacecraft at 1/10th the dry mass of conventional torque rods and reaction wheels.[1] Eventually, these thrusters are designed for primary and attitude control propulsion on future 25-kg class spacecraft performing missions such as formation flying space based surveillance and on-orbit satellite servicing. Due primarily to the elimination of the ignitor and corresponding circuit, the MicroPPTs have realized mass reductions from the standard LES 8/9[1,2] PPT of 60-90%, depending on the specific design.

A version of the AFRL MicroPPT[3] is currently in advanced engineering development for the TechSat21 flight scheduled to launch in 2004.[4,5] TechSat21 will use a 200 W Hall thruster as primary propulsion and will include an array of flight sensors[5] designed to assess interactions between the thrusters and the spacecraft. A primary concern for any spacecraft propulsion system, including the MicroPPT, is spacecraft contamination. For a fully developed propulsion system, the contamination effects are mitigated by fully

---

*Ph.D. Candidate, Department of Aeronautical and Astronautical Engineering, Urbana, IL 61801
** Professor, Department of Aeronautical and Astronautical Engineering, Urbana, IL 61801.
‡Scientist, Air Force Research Laboratory.

characterizing the thruster and exhaust plume in laboratory facilities. This data is then used to develop a generic computational model for the thruster. The thruster model is then used to predict the spacecraft interactions expected as a result of using the thruster in space. Finally, the thruster model is validated through flight data with appropriate sensors. The density measurements presented in this paper are a key part of the laboratory data needed to develop a MicroPPT thruster and plume model. The model development will be accomplished at the University of Michigan under Boyd and Keidar.

The AFRL MicroPPT currently in development for TechSat21 uses a 3 electrode configuration.[5] A small diameter rod (center electrode) is encased in a small-diameter annulus of Teflon™, which is then encased in a relatively small diameter tube which acts as the intermediate electrode. This construction is then encased in a second larger diameter annulus of Teflon™, which is then encased in a large diameter outer electrode. The MicroPPT is fired by a low-energy breakdown between the intermediate and central electrode. This discharge provides enough seed ionization to enable the higher energy conduction breakdown between the intermediate and outer electrode. The discharge between the intermediate and central electrode is referred to as the "trigger discharge." The discharge between the intermediate and outer electrode is referred to as the "main discharge."

Although a wide range of parameters are tested in various MicroPPT configurations, typically the trigger discharge will consume about 1/50 the energy of main discharge. In this fashion, the MicroPPT has demonstrated the ability to passively initiate a surface breakdown discharge across outer propellant diameters as high as 1/4" using a relatively low voltage below 3000V. Without the 3-electrode configuration, up to 40 kV would be required to initiate the discharge across a 1/4" diameter. This would place excessive design requirements on the power-processing unit and on the spacecraft EMI shielding.

In this work, research is performed on simple 2-electrode MicroPPT test-bed configurations. Understanding the physical processes in this geometry has proven beneficial in advancing the optimization of the MicroPPT by separating the requirements for the trigger and main discharges. Research[10] on small diameter 2-electrode designs, generally between 1-3 mm, is applicable to the trigger discharge. Research on larger diameter 2-electrode designs, typically between 3 and 7 mm, are more applicable to the main discharge.

The small plasma volume of the MicroPPT creates a significant diagnostic challenge. For material probes, such as electrostatic or magnetic field probes, the characteristic length of the probe is comparable to or larger then the MicroPPT plasma volume.[6] For interferometric techniques to measure density,[11] the measurement resolution is constrained by the short scale length of the plasma. Since the interferometer measures a phase shift proportional to the product of the density and the laser path length through the plasma, the fundamentally short path length results in excessive measurement uncertainty for the line-averaged plasma density.

To address this problem, a Herriott Cell[7] interferometer was used and a technique employing a 'point measurement'[8] was developed. This technique converges multiple laser passes in a Herriott Cell down to a small area, thereby providing increased laser path length within the plasma. This has the effect of increasing instrument resolution with minimal impact on the spatial resolution.

The Herriott Cell has also been used to combat the effects of mechanical vibrations on interferometric measurements.[9] Vibrations cause physical path length changes through motion of optical components, thereby increasing measurement uncertainty that can mask actual density measurements. While electron density can be separated from this effect through the use of a 2nd laser frequency, neutral density measurements remain susceptible, especially at late times. The increased laser path length acts to overcome the vibrational contribution and increase the signal-to-noise ratio of the neutral vapor. Efforts to measure the neutral density after the current pulse using this technique are discussed here.

During the pulse, electron and neutral density are separated by means of a 2nd laser frequency for comparison with Herriott Cell

measurements. A calculation of the ionization fraction from these measurements is performed and discussed here.

Visual observation of the testbed and MicroPPTs indicate that current spoking is a common occurrence in both devices. While the discharge location tends to remain in approximately the same azimuthal location during a single discharge pulse, sporadic movement of the azimuthal location is observed for subsequent discharges. The effect that this current spoking has on the repeatability of the density measurements is considered herein.

The most significant result of this effort is a comparison of the measured electron density with that predicted numerically by Keidar. Very good agreement is observed between the two methods, indicating the robustness of the Keidar model in simulating the electron density component of the MicroPPT exhaust.

Experimental Apparatus

The AFRL electric propulsion facilities at Edwards AFB were used for these experiments. Chamber 5A is well suited for optical diagnostic access to low power electric thrusters. The chamber is 2.1 m^3 and evacuated by 2 Varian 182 4400 Watt diffusion pumps backed by a rotary mechanical pump. Base pressures of ~30 μTorr are typical. The chamber is electrically floating to eliminate plasma current conduction to the walls. Optical access is available through several 14-inch quartz viewports.

AFRL Micro-PPT Testbed

Data is taken on a testbed similar in design to a MicroPPT. The MicroPPT testbed uses a coaxial geometry with bare copper outer anode and central cathode that is silver-coated copper. The outer diameter of the thrusters tested here is 6.35 mm while the outer Teflon™ diameter is 5.46 mm. The cathode diameter is 1.64 mm. A DC-DC converter charges a 0.417 μF capacitor to 5.6 kV, corresponding to a stored energy of 6.6 J. Figure 1 shows a schematic of the MicroPPT testbed design used for this experiment. Not shown in Fig. 1 is the external sparkplug used to initiate the discharge in the testbed configuration. A 0.5" diameter plug is placed approximately 2 cm from the propellant face, at a 45 degree angle, and discharged with a 0.5 J capacitor that is triggered from the data acquisition system.

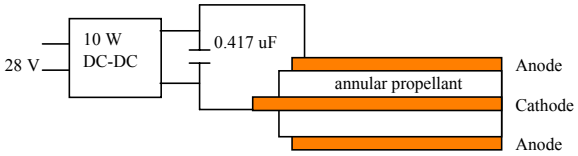

Figure 1: AFRL MicroPPT testbed schematic.

Interferometer Layout

The interferometer employs quadrature heterodyning technique and a Herriott Cell for increased path length exposure. Detailed descriptions of these are given elsewhere.[9,11]

Figure 2 gives a general layout of the interferometer with the second laser frequency option. A Bragg cell splits the 150 mW Argon-ion laser (488 nm) into scene and reference beams using a 40 MHz shift in the reference beam. The scene beam is directed into the vacuum tank through a quartz viewport and into the Herriott Cell optics. The Herriott Cell optics for the point measurement configuration require the Herriott Cell mirrors as well as focusing and guiding optics for the input and exit beams. The MicroPPT is situated halfway between the Herriott Cell mirrors.

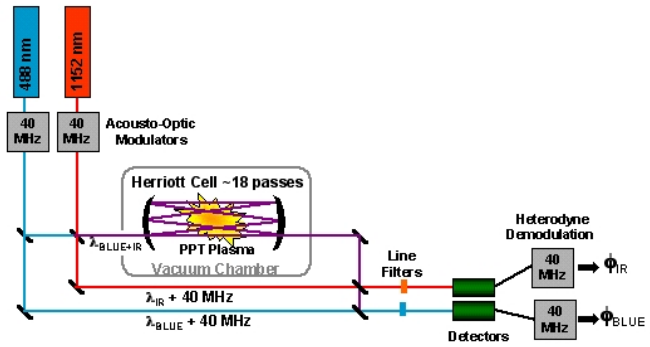

Figure 2: Interferometer Layout.

The scene beam is then returned to the external optics table and recombined with the reference beam that travels the same path length. The combined beams are focused on the detector for optimal measurement intensity.

Herriott Cell Interferometer

The Herriott Cell holds a two-fold advantage over a standard single-pass interferometer. First, it increases sensitivity to plasma-induced phase shifts almost linearly with the number of reflections in the cell. This means that total uncertainty measured during a pulse is decreased. Second, over long timeframes (t > 50 μs) the Herriott Cell increases the signal-to-noise ratio of the neutral density signal which has previously enabled density measurements of late-time neutral vapor emitted from the Teflon™ face.[8,9]

The expected phase shift due to the plasma generated is written as (MKS units, radians)[11]

$$\Delta\phi = 2.8\times10^{-15}\lambda\int n_e dl - \frac{3.9\times10^{-29}}{\lambda}\int n_n dl \qquad (1)$$

where λ is the laser wavelength, n_e is the electron density, and n_n is the neutral density. An assumption concerning the characteristic path length is made here to convert the calculations to common density units. In this case, the diameter of the thruster is used to define the distance over which each laser reflection experiences a phase shift. Line integration over the characteristic path length then allows equation (1) to be rewritten as

$$\Delta\phi = 2.8\times10^{-15}\lambda N n_e l - \frac{3.9\times10^{-29} N n_n l}{\lambda} \qquad (2)$$

where N is the number of reflections in the Herriott Cell and l is the characteristic path length (0.00635 m). For a given density, an increased number of passes results in a linearly higher phase shift in the scene beam, thereby increasing the resolution of the instrument.

A third term may be added here to account for physical path length changes due mainly to mechanical vibration sources. This can be written as

$$\phi_{PL}(t) = \frac{2\pi\Delta l}{\lambda} \qquad (3)$$

where Δl is the total physical movement of the optics. It is apparent that for a given measured phase shift, the vibrational term has no dependence on the number of passes. The consequence is that normally intrusive vibration measurements can be overcome by increasing sensitivity to neutral density in the Herriott Cell technique.

Advantages of Herriott Cell measurements on standard parallel plate and coaxial PPTs have previously been demonstrated.[9] The present concern rests on the ability of the Herriott Cell to provide increased instrument sensitivity in a "point measurement" configuration. The point measurement mode of operation directs increasing number of laser beam reflections within a 3-mm spread. Figure 3 shows an optical ray tracing simulation of the point measurement using the commercial BEAM 3 software package.[12] In Fig. 3, note that the diameter of the laser beam, and the diameter of the convergence point is on the order of the size of the MicroPPT and the spatial extent of the plasma under investigation. Therefore the interferometer cannot resolve the spatial distribution of the plasma density. Instead, the enhanced sensitivity is used to enable a measurement of the total plasma density near the thruster exit plane, and this value is used in the comparison to the MicroPPT plume model.

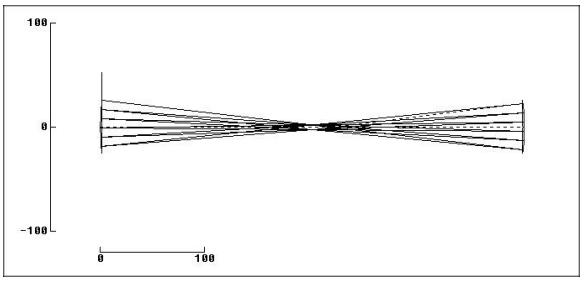

Figure 3: Optical ray tracing of the point measurement beam geometry.

Requirements for this beam geometry include extra optics not required for the previously used planar geometries. Two additional optics are required in the tank, including a lens on the entrance to the cell that must focus the incoming beam at the center of the cell, and an elliptic pick-off mirror to direct the final reflection out of the cell. A schematic of the in-tank optical setup is shown in figure 4.

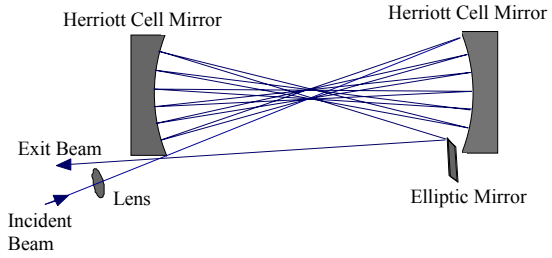

Figure 4: Schematic of in-tank optics required for the 'point' measurement technique.

The cell design includes 2 spherical mirrors of 50.8-mm diameter with focal lengths of 101.6-mm. These mirrors are coated with UV Enhanced Aluminum for good broadband reflectivity (>90% for 450-1200 nm). The entrance lens is an f/# 9.8 achromatic lens of 25.4-mm diameter and the pick-off mirror is an elliptical mirror coated with Protected Silver (>96% for 480-1200 nm). The Herriott Cell mirrors are separated by twice the radius of curvature (406.4 mm) and the incoming beam is focused at the halfway point. Control over the number of passes is exercised using mirror tilt and entrance angle. For this experiment, 13 passes are used, giving a beam intensity ratio of $(0.9)^{13} = 0.25$.

Apparent in the beam traces of Fig. 4 is the existence of 2 closely spaced convergence points, separated by 3-5 mm depending on test configuration. One of the points contains 7 of the laser passes and the other contains 6. Data reduction is generally performed using N=13, where the density is then averaged over the 2 convergence points. Single point beam convergence appears to be unachievable with the Herriott Cell, with the exception of the simple two pass limiting case.

This configuration can be used experimentally in two possible modes. Assuming a vertical focal plane for the beams, the first mode fires the microthruster perpendicular to the focal plane across both convergence points causing a loss in radial spatial resolution of the plasma. By firing the microthruster parallel to the focal plane, the device increases radial spatial resolution at the expense of axial resolution. Figure 5 shows the beam pattern over the fuel face for the former case.

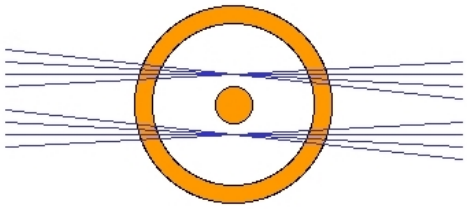

Figure 5: Schematic showing fuel face coverage when firing the thruster perpendicularly across the plane of the focal points.

Validation of this technique using the two focal points requires demonstration of self consistent measurements throughout the plasma and agreement with measurements taken by proven devices. To achieve this, measurements are taken at 1-mm and 5-mm axially distant from the fuel face. At both positions, measurements are taken in the configuration shown in figure 8. The foci that is on the thruster centerline is then moved up 3 mm such that it now measures density where the outer foci was. This stepping is continued until the outer foci is at a 9-mm radius from the thruster centerline. These measurements are compared and used to create a 2-dimensional contour plot of the electron density for analysis of self-consistency. Density measurements are also taken with a two-color interferometer to demonstrate what effect, if any, curved reflective surfaces have on the measurements.

Two-Color Interferometer

A two-color interferometer was also constructed for baseline comparison of electron and neutral densities. This interferometer allows separation of electron and neutral densities throughout the pulse. A 488-nm Ar-ion laser was used simultaneously with an 1152-nm HeNe laser providing direct measurements of both electron and neutral densities early in the pulse. This data is taken at 5-mm distance from the fuel face and provides the control case for density measurements with the Herriott Cell. The electron and neutral densities are calculated from

$$n_e = \frac{\Delta\phi_r \lambda_r - \Delta\phi_b \lambda_b}{-2.8 * 10^{-15} Nl\left[\lambda_r^2 - \lambda_b^2\right]} \qquad (4)$$

$$n_n = \frac{\frac{\Delta\phi_r}{\lambda_r} - \frac{\Delta\phi_b}{\lambda_b}}{3.9 * 10^{-29} Nl\left[\frac{1}{\lambda_r^2} - \frac{1}{\lambda_b^2}\right]} \qquad (5)$$

where λ_r and λ_b are the infrared and blue laser wavelengths (m) respectively, $\Delta\phi_r$ and $\Delta\phi_b$ are the measured phase shifts for the infrared and blue lasers (radians), N is the number of passes through the plasma experienced by the scene beams, and l is the characteristic length (m).

Experimental Results

The baseline data from the two-color interferometer shows electron and neutral density at 5 mm from the fuel face for 6.6 J discharge and 2 passes. Figure 6 shows this data for the first 30 µs after the discharge. Peak electron density reaches $2\pm0.2 \times 10^{16}$ cm^{-3}.

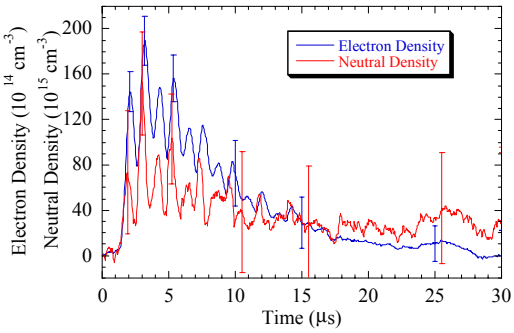

Figure 6: Electron and Neutral Densities separated by two-color interferometry. 2 passes at 5 mm from fuel face, 6.6 J.

Electron density for a 13 pass case are shown at a distance of 5 mm from the fuel face and 6.6 J in figure 7. Also shown are measurements taken without firing the thruster showing the effects of mechanical vibration throughout this timeframe. Both sets of data are calculated by averaging 20 data shots.

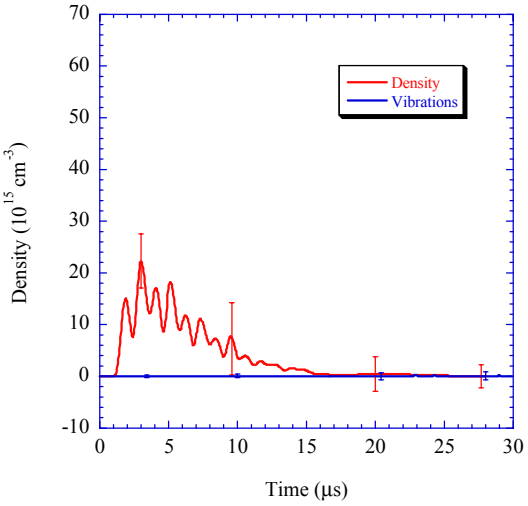

Figure 7: Electron density with vibrations for 13-pass beam geometry shown in Figure 8. 5mm from fuel face and 6.6 J.

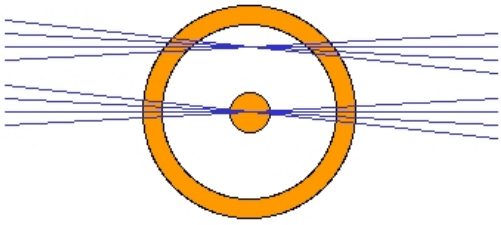

Figure 8: Schematic showing fuel face coverage for data in figure 7.

Figure 8 illustrates the beam geometry over the fuel face. In this geometry, 7 reflections of the 13 pass directly in front of the center electrode while the remaining 6 reflections pass in front of the Teflon™ surface. Peak electron density reaches $22\pm8 \times 10^{15}$ cm^{-3}.

Also for comparison, figure 9 shows electron density for the case of both convergence points passing in front of Teflon™ instead of the electrode. The beam geometry for this case is shown in figure 5 and peak electron density is $2.8\pm0.22 \times 10^{16}$ cm^{-3}. This case is plotted with the current waveform.

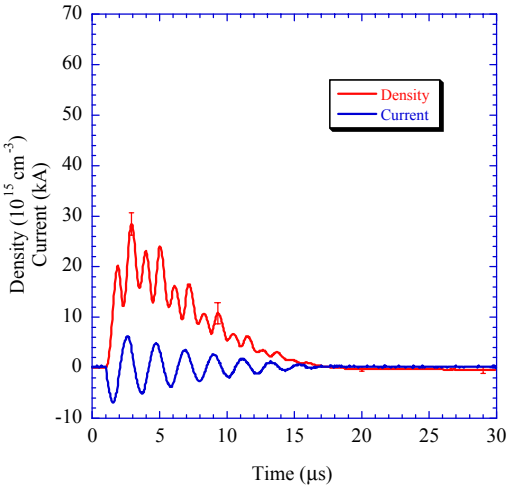

Figure 9: Electron Density with current for 13 pass configuration shown in Figure 5 at 5 mm from fuel face and 6.6 J.

Figure 10 shows electron density for the 2-color 2-pass configuration co-plotted with the electron density from figure 7.

The close agreement between the two-color measurement and the Herriott Cell measurement suggests that the geometry and optics involved in the Herriott Cell technique do not negatively affect the diagnostic.

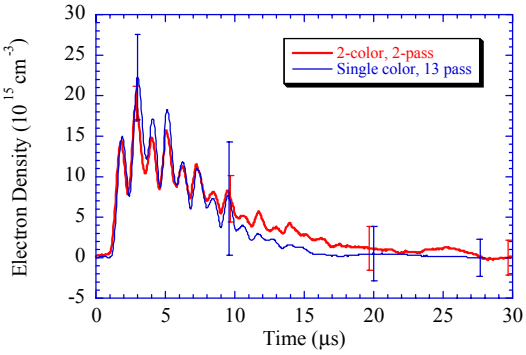

Figure 10: Comparison of 2-color electron density measurement to 13-pass measurement in Fig. 8. Both measurements taken 5 mm from fuel face.

Polarity Effects

Electron density measurements in this effort are generally acquired with the center electrode charged positive and the outer electrode grounded. Figure 11 shows the electron density waveforms for this positive polarity case, along with the discharge current waveform. The structure of the peaks in the electron density is similar for all data acquired for the positive polarity case.

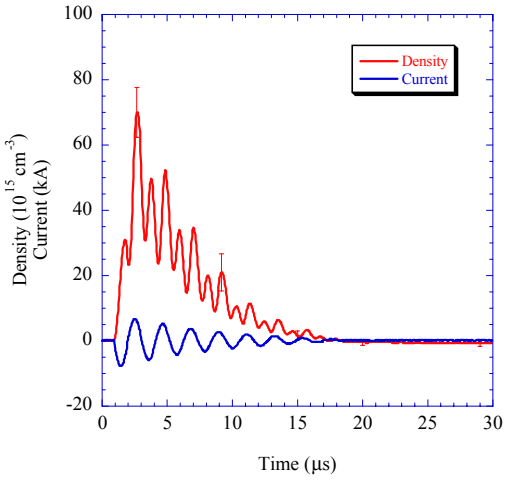

Figure 11: Positive polarity discharge. 13 passes, 1 mm from fuel face, 7.5 J.

Figure 12 shows the negative polarity case where the outer conductor is still grounded, but the center electrode is now charged to a negative potential.

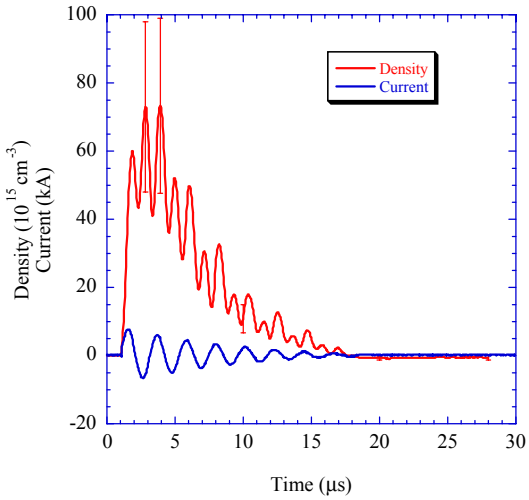

Figure 12: Negative polarity discharge. 13 passes, 1 mm from fuel face, 7.5 J.

A significant increase in measurement uncertainty is observed in this case due to larger shot-to-shot variation of the measured density. The general structure of the peaks in the electron density waveforms is observed in each individual firing. In both cases, the data are acquired at 7.5 J, 1 mm from the fuel face and the plots in Figs 11 and 12 are an average of 9 and 15 shots respectively.

Electron Density Mapping

A significant amount of data was taken to determine whether the two focal points inherent in the point measurement would affect the integrity of the diagnostic. Figure 13 shows the location of focal points with respect to the exit plane of the thruster for the purpose of counting out from the external measurement points. This figure shows a cutaway of half the thruster with the diamonds representing focal points. Pairs are located at y = 0 and 3, y = 3 and 6, and y = 6 and 9 mm. Another pair is taken behind the exit plane of the thruster at x = -1 and-4 mm. For consistent representation of these data, the thruster body is given a value of 0 density. Also, x=1, y=9 is given a value of zero density. This was not measured, but is consistent in terms of the measurements and focal point locations.

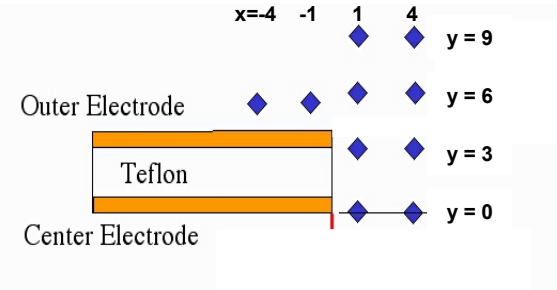

Figure 13: Location of Herriott Cell focal points for the test matrix with cutaway from centerline to maximum radius.

Figure 14 shows the result of this data for peak electron density at t=2 μs. This plot must be understood in terms of the following information. The thruster exit plane marks the x=0 position. Density was set to zero at the thruster exit plane.

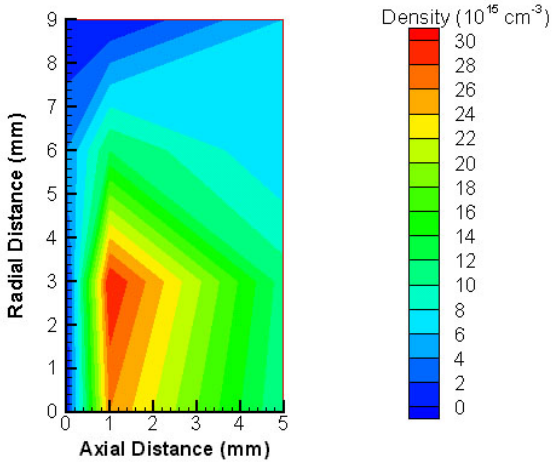

Figure 14: Peak electron density (t = 2 μs) in terms of axial and radial distance. Actual data points are shown in figure 13 with linear interpolation between data points. y=0.82 is the radius of the center electrode, y=3.18 is the outer electrode radius.

Actual data points were taken at x=1 and 5 mm and y = 0, 3, 6, and 9 mm. External density data taken at 1 mm behind the exit plane was used at point (0, 6) for consistency. The graphics program performs a linear interpolation between the data locations to construct the contour plots. Therefore this graphical representation should be taken as a rough attempt to compare model predictions with electron density measurements in several locations.

External Density Measurements

Density measurements are taken alongside the outer electrode with the 13-pass configuration. The focal point with 7 passes is located 1 mm behind the exit plane of the thruster. The focal point with 6 passes is located 4 mm behind the exit plane of the thruster. Both focal points are 1 mm radially outside the outer electrode. Figure 15 shows a peak electron density of $4\pm2\times10^{15}$ cm^{-3} for this case.

The presence of electron density behind the exit plane of the thruster is also supported by data from an originally unrelated experiment. The tip of the MicroPPT is coated with barium hydroxide, which is allowed to dry on the surface. This was done for emission spectroscopy purposes.

After firing for ~600 shots, photos were taken showing the recession of barium powder from the thruster tip. Figure 16 shows pictures of the barium-covered thruster both before and after firing.

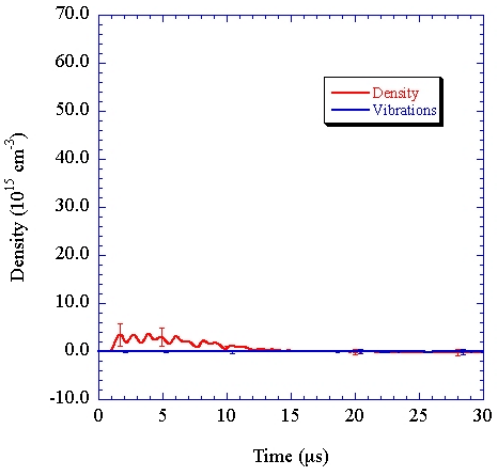

Figure 15: Electron density data taken external to the outer electrode (alongside).

Measurements taken around the thruster annulus show the barium recedes from the end of the thruster between 1.5 – 3 mm, suggesting current attachment on the outside of the outer diameter. The presence of plasma density in the backplane of the thruster was also predicted in the modeling efforts of Boyd and Keidar.[13]

Figure 16: MicroPPT coated with barium hydroxide pre-firing (left) and after ~600 shots (right).

Neutral Density Measurements

Using the point measurement technique, the uncertainty effects of vibrations are increased and practical limits arise with increased passes. A primary reason that vibrations effects are increased is that relative motion of the lens, shown in Fig. 4 has the undesired effect of magnifying the vibrational displacement of the laser beam. The practical limit is that the lens introduces a convergence and divergence of each beam as it traverses the region between the mirrors. This has the undesired effect of magnifying the beam expansion, making it difficult to align the entire beam on the elliptic pickoff mirror in Fig. 4, and limiting the number of passes that can be accomplished. Due to these limitations, discernible neutral density measurements were not obtained at any point in the pulse with the Herriott Cell. Two-color interferometry in a simple 2-pass configuration did allow neutral measurements for t < 20 μs, but after that period vibrational noise exceeded the neutral density signal.

Figure 17 shows the two-color data with typical error bars taken at 5 mm from the fuel face. Figure 18 shows the same measurement using the 13 pass Herriott Cell.

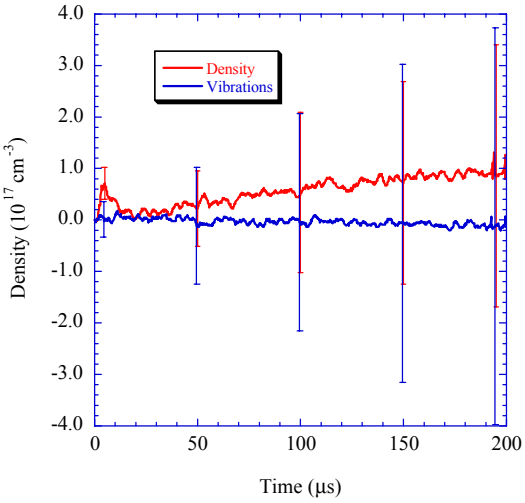

Figure 17: Neutral density measurements from 2-color, 2 pass interferometry. Data taken at 5 mm from the fuel face for a 6.6 J discharge. Typical error bars shown.

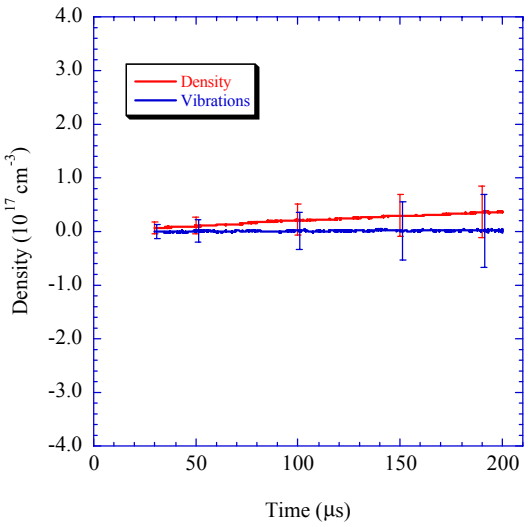

Figure 18: Neutral density measurements from 13 pass Herriott Cell interferometry. Data taken at 5 mm from fuel face as shown in figure 5 for 6.6 J discharge. Typical error bars shown.

Data starts at 30 μs for this case because it is a single laser measurement and data before 30 μs is reduced for electron density. After 30 μs, electron density is gone yielding a measurement of neutral vapor and mechanical vibrations. The error bars are determined by the standard deviation of 20 firings in each case.

Comparison of figures 17 and 18 shows a significant uncertainty decrease due to the increase in laser passes in the Herriott Cell. Data does show that at 200 μs after the discharge, neutral density is no larger than 8.5×10^{16} cm^{-3}.

Discussion of Results

Thruster and Model Comparisons

A significant finding of this experiment is the degree of agreement between theoretical modeling predictions and experimental results. A basis for comparison is required for some modeling and data performed for systems that are not similar in energy or dimension. Definition of the energy-to-area ratio provides such a basis and is used here to investigate the comparison between past and current predictions and measurements.

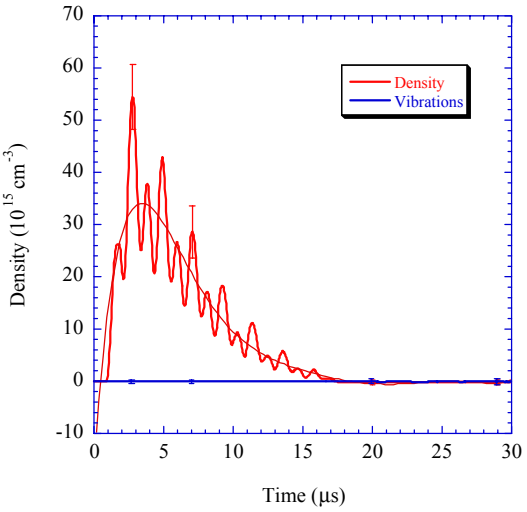

Figure 19: Electron Density with vibrations for 13 pass configuration shown in figure 5 at 1 mm distant from fuel face. A 7th order polynomial curve is fit to the electron density curve.

Comparison of electron density peaks from various sources can be made if input energy and fuel surface area are known. Table 1 shows a comparison of data with past predictions made by Keidar concerning MicroPPT electron density.

The current experiment uses a 6.35-mm diameter MicroPPT. Figure 19 shows electron density data with a 7th order polynomial curve fit.

Keidar and Boyd[13] predict electron density using a hybrid fluid-PIC-DSMC approach. The energy-to-area ratio for this model is higher than that of the experimental setup used. This is balanced by increased electron density. Both the raw data density peak and the curve-fit peak are compared to Keidar's predictions concerning a smaller diameter MicroPPT. The last column in table 1 shows peak electron density divided by the energy-to-area ratio. This ratio shows strong agreement for both experimental cases with Kiedar's model.

Table 1: Data parameters for thruster comparisons.

Case	E/A (J/mm^2)	Peak n_e (10^{15} cm^{-3})	Energy (J)	Capacitance (μF)	Distance from Fuel Face (mm)	(Peak n_e) /(E/A)
6.35 mm MicroPPT raw data	0.31	55	6.6	0.417	1	177
6.35 mm MicroPPT curve fit	0.31	35	6.6	0.417	1	113
3.1 mm Keidar Model[13]	8.4	1000	15.2	0.3	1	119

Predictions made by Keidar for the 6.35-mm diameter MicroPPT show strong agreement with experimental data. Description of the model is given elsewhere.[14] Figure 20 shows direct comparison of predicted electron density using an experimental current waveform as input.

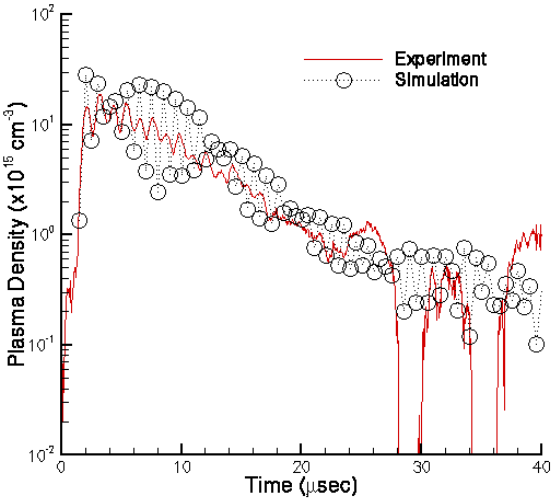

Figure 20: Comparison of predicted and measured electron density time variation at 5 mm from the propellant face at the axis in the case of 6.35-mm diameter MicroPPT firing at 6.6 J.
The solid line shows density measured using the Herriott Cell. The degree of agreement is apparent, and provides support for the model being developed.

Polarity Effects

There is a noticeable difference in the electron density measurements for both thruster polarities. For positive polarity (central electrode charged positive, outer electrode at electrical ground) the first peak in density is smaller than the second, and every odd numbered peak is smaller than its predecessor. For negative polarity, there is a substantial increase in first peak density and every odd numbered peak is approximately the same magnitude as or larger than its predecessor. This effect is commonly witnessed in MicroPPT operation and is attributed to the coaxial geometry. The dominant effect here is electrons emitted from the cathode via field emission to complete the current path. A stronger electric field abets field emission. The electric field is stronger in the regions of high curvature near the center conductor. Therefore when the inner conductor is the cathode, electron emission is enhanced, and the effective impedance of the circuit is reduced leading to higher current.

Ionization Fraction

From 2-color data, a calculation of the ionization fraction, α, can be performed assuming single ionization. Figure 21 shows the results of this calculation according to equation 6 below.

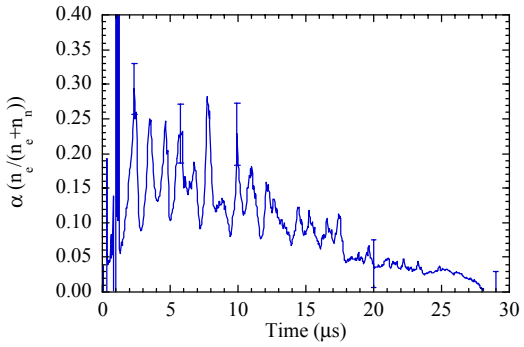

Figure 21: Ionization fraction α, calculated from the separation of electron and neutral density in Fig. 6. The large peak at t = 1μs is due to signal noise.

$$\alpha = \frac{n_e}{n_e + n_n} \qquad (6)$$

The oscillations in α occur at double the frequency of the current. Also, the current ends at 17 μs while there remains ~4% ionization fraction until 28 μs after the discharge. On average, α decreases smoothly from 18% down to 9% when the current ends.

External Electron Density

Figures 15 and 16 give strong evidence of plasma presence as much as 3 mm behind the exit plane. Keidar and Boyd predict non-zero carbon ion densities at the exit outside a 3.1 mm diameter MicroPPT.[13] Plasma backflow and external arc attachment can explain this phenomenon.

Conclusions

Agreement between present electron density measurements and predictions by Keidar is strong. Comparison by the energy-to-area ratio argument for the 3.1-mm MicroPPT matches well using curve-fit data taken here. Also, specific predictions using the current waveform as an input followed measured electron densities very closely. This indicates some level of validation for Keidar's theory.

The agreement between 2-color and Herriott Cell electron density data shown in figure 10 is strong, suggesting that the 'point' measurement technique is valid. Differences in uncertainty are probably due to shot-to-shot variations in thruster firing. One noticeable result over long timeframes is that the extra optics for focusing and beam pick-off increase vibrational uncertainty.

A large amount of data at various locations was taken to demonstrate consistent measurements using the two focused points inherent in the 'point' measurement technique. This data appears self consistent as demonstrated in figure 14.

Thruster polarity has some effect on the electron density peak structure, but does not completely account for the low first peak witnessed in all MicroPPT data. This is possibly attributable to residual ionization in the plasma between current oscillations, enhancing the ionization process and lowering the effective impedance for successive current oscillations.

Electron density is measured outside the annular electrode at 1 mm behind the exit plane with a peak of $4\pm2\text{x}10^{15}$ cm^{-3}. Barium hydroxide erosion back from the exit plane over a large number of firings corroborates the measurement. This is in agreement with Keidar's predicted ion densities.

Attempts to measure neutral density with the increased resolution of the interferometer were unsuccessful. For standard PPTs, the Herriott Cell has been effective in measuring neutrals as late as 200 μs after the pulse for single shots, with averaged neutral density measured out to 150 μs.[8] However, previous measurements used the Herriott Cell without external focusing optics and were therefore less susceptible to mechanical vibrations late in time. Past measurements also used higher numbers of passes in the Herriott Cell that are not achieved here. A neutral density upper limit of $8.5\text{x}10^{16}$ cm^{-3} at 200 μs after the pulse is established and there is significant reduction in uncertainty using the multiple pass technique.

Neutral density from two-color interferometry early in the pulse was used with electron density to calculate the ionization fraction, α. This calculation assumes single ionization, a tenuous assumption in these devices.

Acknowledgements

This work was partially funded by the Air Force Office of Scientific Research. M. Birkan is the Program Monitor. The authors would like to thank D. White, J. Schilling, and S. Bushman of W.E. Research for technical assistance. E. Antonsen acknowledges dual support from the University of Illinois at Urbana-Champaign and the AFRL through Spiral Technologies.

References

1. M.L. McGuire and R.M. Myers, "Pulsed Plasma Thrusters for Small Spacecraft Attitude Control," GSFC Flight Mechanics/Estimation Theory Symposium, May 13-16, 1996.

2. R.J. Vondra, "The MIT Lincoln Laboratory Pulsed Plasma Thruster," AIAA Paper No. 76-998, Nov. 1976.

3. G.G. Spanjers, D.R. Bromaghim, D. White, J. Schilling, S. Bushman, J. Lake, M. Dulligan, "AFRL MicroPPT Development for the TechSat21 Flight," 27th Intl Electric Propulsion Conference, IEPC paper 2001-166, Pasadena, CA 2001.

4. D.R. Bromaghim, G.G. Spanjers, L.K. Johnson, R. Gorecki, D. Tan, R. Vondra, B. Pote, J. Barbarits, "The AFRL TechSat21 Propulsion Subsystem Development Program," 27th International Electric Propulsion Conference, IEPC paper 2001-165, Pasadena, CA 2001.

5. L.K. Johnson, D. Conroy, G.G. Spanjers, and D.R. Bromaghim, "Propulsion Instrumentation for Small Hall Thruster Integration," 27th International Electric Propulsion Conference, paper IEPC-01-167, Pasadena, CA 2001.

6. G.G. Spanjers and R.A. Spores, "PPT Research at AFRL: Material Probes to Measure the Magnetic Field Distribution in a Pulsed Plasma Thruster," 34th AIAA Joint Propulsion Conf, paper AIAA-98-3659, Cleveland, OH, July 12-15, 1998.

7. D.R. Herriott, H. Kogelnik, R. Komfner, "Off Axis Paths in Spherical Mirror Interferometers," *Applied Optics*, 3, 1964, 523.

8. E.L. Antonsen, R.L. Burton, S.F. Engelman, G.G. Spanjers, "Herriott Cell Interferometry for Unsteady Density Measurements in Small Scale Length Thruster Plasmas," AIAA Paper No. 2000-3431, July 2000.

9. E.L. Antonsen, *Herriott Cell Interferometry for Pulsed Plasma Density Measurements*, MS Thesis, University of Illinois at Urbana-Champaign, 2001.

10. F.S. Gulczinski III, M.J. Dulligan, J.P. Lake, G.G. Spanjers, "Micropropulsion Research at AFRL," AIAA Paper No. 2000-3255, July 2000.

11. G. G. Spanjers, K. A. McFall, F. S. Gulczinski, R. A. Spores, "Investigation of Propellant Inefficiencies in a Pulsed Plasma Thruster," AIAA Paper No. 96-2723, July 1996.

12. Stellar Software, Berkeley, CA, **www.stellarsoftware.com**

13. M. Keidar, I.D. Boyd, "Electromagnetic Effects in the Near Field Plume Exhaust of a Pulsed Plasma Thruster," AIAA Paper No. 2001-3638.

14. M. Keidar, I.D. Boyd, F.S. Gulczinski III, E.L. Antonsen, G.G. Spanjers, "Analyses of Teflon™ Surface Charring and Near Field Plume of a Micro-Pulsed Plasma Thruster," 27th Intl Electric Propulsion Conference, IEPC Paper 2001-155, Pasadena, CA 2001.